

Cooperative Multi-Satellite ISAC Networks: Centralized vs. Distributed Sensing

Jeongbin Kim, Jaehong Jo, Seunghyeon Jeon, Yo-Seb Jeon, *Member, IEEE*,
Wonjae Shin, *Senior Member, IEEE*, and H. Vincent Poor, *Life Fellow, IEEE*

Abstract—This paper investigates a downlink multi-satellite integrated sensing and communication (ISAC) network, in which multiple satellites simultaneously transmit ISAC signals to provide communication services to ground user equipments and enable cooperative sensing of airborne targets through multiple gateways. To support this dual functionality, we introduce communication and sensing beamforming designs based on uniform planar arrays with optimized power allocation. Building on these designs, we propose two cooperative sensing frameworks, namely centralized and distributed. In the centralized framework, each gateway forwards its sensing observations to a central unit (CU), where the positions of multiple targets are jointly estimated from the aggregated data using a sparse signal recovery formulation. To mitigate the signaling overhead inherent in centralized processing, a distributed framework is further proposed, in which each gateway independently estimates target positions and transmits only the local estimates to the CU. To associate estimates from different gateways, a data association problem based on the squared Euclidean distance is formulated and efficiently solved using the Hungarian algorithm. The final target positions are then obtained by minimizing the distance estimation error. Simulation results demonstrate that the proposed centralized and distributed frameworks significantly outperform existing sensing schemes while satisfying communication performance requirements. We also evaluate the sensing-communication trade-off from the viewpoints of sensing accuracy and communication power consumption under the proposed frameworks.

Index Terms—Integrated sensing and communication (ISAC), cooperative sensing, centralized sensing, distributed sensing, multi-satellite network.

I. INTRODUCTION

Satellite systems have attracted considerable attention as a key technology in 5G and beyond-5G wireless networks for supporting ubiquitous and global connectivity [1], [2]. This evolution has been further supported by the standardization efforts of the 3rd Generation Partnership Project (3GPP), which has incorporated non-terrestrial networks (NTNs) into enhanced mobile broadband and machine-type communication frameworks [3]. Nevertheless, the overall system performance of an individual satellite is inherently limited by constrained onboard power budgets and processing capabilities, which hinder its ability to meet the demands of NTNs in terms of throughput,

latency, and reliability. To overcome these bottlenecks, cooperative satellite systems have been introduced, which are expected to provide low-latency and ultra-reliable communication services with seamless coverage via inter-satellite cooperation [4]. Recently, the deployment of low Earth orbit (LEO) satellites has accelerated the growth of dense and large-scale satellite networks [5]. Building upon this infrastructure, LEO satellites have expanded their utility beyond connectivity to support a wide range of services, including Earth monitoring, positioning, and navigation [6]. However, the advancement of LEO satellite systems toward dual roles in communication and sensing has inevitably introduced new challenges associated with orbital and spectral constraints, such as spectrum congestion, inter-satellite interference, and complex constellation design [7].

Integrated sensing and communication (ISAC) has been considered a promising technology for future wireless networks due to its unified signal processing and common hardware for communication and sensing. This integration simultaneously provides wireless communication and sensing within a shared spectrum and thus achieves reduced hardware cost, improved spectral efficiency, and mitigated spectrum conflicts [8]. In a cell-free multiple-input multiple-output (MIMO) system, multiple ISAC transceivers can collaborate to perform multistatic sensing and jointly serve communication users for enhancing sensing robustness and communication reliability over wide areas [9]. Motivated by this, multi-satellite ISAC networks have been studied to facilitate high-accuracy sensing and reliable communication with global coverage. Nevertheless, multi-satellite ISAC networks still face technical challenges for practical realization, which mainly lie in the design of cooperation frameworks.

The cooperative ISAC networks can be categorized into two types based on their cooperation level, namely centralized and distributed frameworks [10]. The centralized framework jointly processes all observations from the spatially distributed sensor network. In contrast, the distributed framework consists of weak cooperation, in which each sensor independently performs local sensing and shares its results for subsequent fusion to improve accuracy. While centralized frameworks can achieve high sensing accuracy by fully exploiting global information, they generally require considerable fronthaul capacity and computational resources at a central unit (CU), which may limit their scalability and practical deployment. On the other hand, distributed frameworks significantly reduce fronthaul overhead and computational burden by relying on local processing, at the cost of potentially degraded sensing performance due to limited

Jeongbin Kim, Jaehong Jo, Seunghyeon Jeon, and Yo-Seb Jeon are with the Department of Electrical Engineering, POSTECH, Pohang, Gyeongbuk 37673, South Korea (e-mail: jb2067@postech.ac.kr; jaehongjo@postech.ac.kr; seunghyeon.jeon@postech.ac.kr; yoseb.jeon@postech.ac.kr).

Wonjae Shin is with the School of Electrical Engineering, Korea University, Seoul 02841, South Korea (email: wjshin@korea.ac.kr).

H. Vincent Poor is with the Department of Electrical Engineering, Princeton University, Princeton, NJ 08544 (e-mail: poor@princeton.edu).

information exchange. This trade-off between sensing accuracy, communication overhead, and implementation complexity motivates a systematic investigation of cooperative frameworks in multi-satellite ISAC networks.

A. Related Works

1) *Cooperative Terrestrial ISAC*: Most existing studies on cooperative sensing have been conducted in terrestrial scenarios. For example, the studies in [11], [12] investigate centralized sensing frameworks, where observations collected from multiple nodes equipped with uniform linear arrays are jointly processed at a CU for target detection. Specifically, the target detection problem is solved via sparse Bayesian learning [11] and iterative node selection and refinement [12]. Other studies investigate distributed sensing frameworks, where each sensing node independently processes its received reflected signals and forwards the extracted information, such as AoA pairs [13] or range information [9], [14], to a CU for joint estimation via data fusion. The authors in [15] propose both centralized and distributed frameworks by considering different backhaul capacity constraints and corresponding information fusion strategies. However, these works primarily target terrestrial sensing scenarios and are not directly applicable to multi-satellite ISAC networks due to the fundamentally different deployment geometry.

2) *Non-Cooperative Single-Satellite ISAC*: Most existing studies on satellite ISAC networks have focused on non-cooperative single-satellite scenarios. In [16], a beam squint-aware hybrid beamforming design was proposed for a massive MIMO system to maximize energy efficiency while guaranteeing sensing performance. Similarly, the authors in [17] investigated ISAC beamforming design in satellite-terrestrial networks by capitalizing on the complementary characteristics of satellite and terrestrial networks. The authors in [18] proposed a rate-splitting multiple access-based precoder that jointly considers communication rate and the Cramér-Rao bound (CRB) of angle of arrival (AoA). In addition, this study presented an AoA estimation method based on the multiple signal classification (MUSIC) algorithm. The authors in [19] designed pilot allocation to balance the trade-off between communication and navigation for orthogonal frequency division multiple access-based delay and Doppler estimation. Unfortunately, the sensing performance of the single-satellite ISAC network is fundamentally limited by the lack of spatial diversity. This limitation highlights the need for cooperative multi-satellite ISAC networks.

3) *Cooperative Multi-Satellite ISAC*: Only a few studies have explored cooperative sensing frameworks tailored to multi-satellite ISAC networks. The total CRB for time difference of arrival estimation in multi-target scenarios was optimized by designing beamhopping and power allocation [20], and beam scheduling and transmit beamforming [21]. These studies focused solely on beamforming design without considering a sensing framework. Another study [22] investigated communication and sensing beamforming to minimize the CRB for angle of departure (AoD) and reflection coefficient estimation.

This study also proposed a particle-swarm-optimization-based centralized location sensing algorithm. Despite these early research efforts, none of the existing works has systematically investigated a multi-target sensing process, which is essential for extending the applicability of satellite ISAC networks. Moreover, an effective distributed sensing framework for multi-satellite ISAC networks remains largely unexplored, despite its potential to overcome the high signaling overhead and limited scalability inherent in centralized cooperation for sensing.

B. Contributions

To fill this research gap, in this paper, we present cooperative multi-target sensing frameworks for multi-satellite ISAC networks, an aspect not investigated in existing studies. In this setup, multiple satellites and gateways are deployed to simultaneously provide communication services to ground user equipments (UEs) and perform airborne target sensing. To this end, we design the communication and sensing beamforming based on the uniform planar array (UPA) structure. For practicality, a hybrid analog-digital beamforming architecture is also considered to reduce power consumption and hardware cost for large antenna arrays. Subsequently, we develop both centralized and distributed sensing frameworks to provide comprehensive insights into cooperation design. We also present an analysis of the two frameworks from the viewpoints of fronthaul overhead and computational complexity. Through extensive simulations, we not only compare the performance of the proposed centralized and distributed frameworks, but also validate the superiority of these frameworks over conventional benchmark schemes. The key contributions of this paper are summarized as follows:

- We introduce novel cooperative sensing frameworks for multi-satellite ISAC networks, where multiple satellites transmit ISAC signals to provide communication services to ground UEs and perform target sensing, while gateways receive reflected signals from the targets for cooperative sensing. For this dual-purpose operation, we propose a hybrid beamforming design that jointly supports sensing and communication, aiming to maximize the signal-to-interference-plus-noise ratio (SINR) while minimizing the communication power under quality-of-service (QoS) constraints.
- We propose a centralized sensing framework, where multiple gateways cooperatively perform sensing by transmitting their local observations to a CU, where all collected data are jointly processed. Based on these aggregated observations, we formulate the multi-target sensing task as a group sparse recovery problem and develop an orthogonal matching pursuit (OMP)-based algorithm for efficient target localization.
- We also propose a distributed framework, where each gateway individually estimates the target positions and forwards its results to the CU. To match the estimates associated with the same target, we perform data association by sequentially applying the Hungarian algorithm.

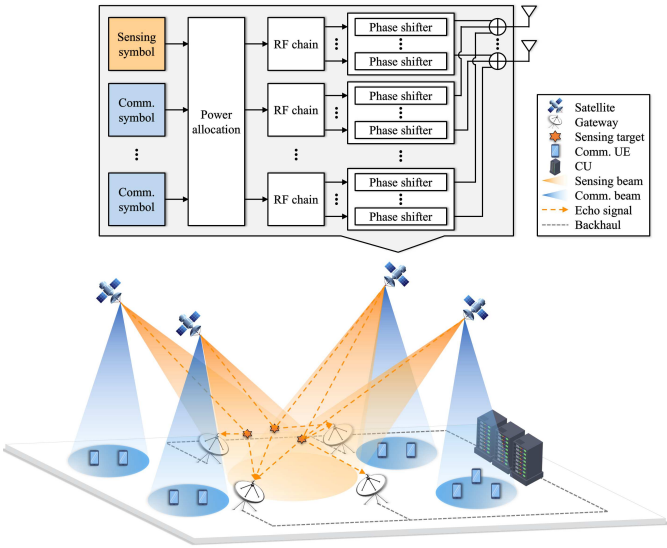


Fig. 1. System model of the proposed multi-satellite ISAC network.

After the association, the target positions are determined by solving a distance error minimization problem with a closed-form solution.

Organization: The rest of the paper is organized as follows. Section II introduces the system model for the considered multi-satellite ISAC network. Section III explains the proposed hybrid analog-digital beamforming design for communication and target sensing. We discuss the centralized and distributed frameworks in Sections IV and V, respectively. Section VI presents numerical results to compare the proposed frameworks. Finally, we conclude the paper in Section VII.

Notations: Scalars, vectors, and matrices are denoted by italic, lowercase boldface, and uppercase boldface letters, respectively. \mathbb{R}^N and \mathbb{C}^N represent the sets of N -dimensional real- and complex-valued vectors, respectively. For a vector \mathbf{x} , \mathbf{x}^T and \mathbf{x}^H denote its transpose and Hermitian transpose; $[\mathbf{x}]_n$ denotes its n -th element, and $\|\mathbf{x}\|_p$ its ℓ_p -norm with $p \geq 0$. For a matrix \mathbf{X} , \mathbf{X}^{-1} and $[\mathbf{X}]_{:,n}$ denote its inverse and n -th column, respectively. The Kronecker product is denoted by \otimes , the magnitude of a complex number by $|\cdot|$, the block diagonal matrix by $\text{blkdiag}(\cdot)$, and the imaginary unit by $j = \sqrt{-1}$. For a set \mathcal{S} , $|\mathcal{S}|$ denotes its cardinality. The N -dimensional zero vector and the $N \times N$ identity matrix are denoted by $\mathbf{0}_N$ and \mathbf{I}_N , respectively. $\mathcal{CN}(\boldsymbol{\mu}, \boldsymbol{\Sigma})$ represents a complex Gaussian random vector with mean vector $\boldsymbol{\mu}$ and covariance matrix $\boldsymbol{\Sigma}$, and \sim indicates that a random variable or vector follows a given distribution.

II. SYSTEM MODEL

Consider a downlink multi-satellite ISAC network, where I satellites and L gateways are deployed to simultaneously provide communication services to ground UEs and perform passive target sensing over T time slots, as illustrated in Fig. 1. Each satellite is equipped with a half-wavelength spaced UPA. The arrays consist of $N^{\text{sat}} = N_x^{\text{sat}} \times N_y^{\text{sat}}$ antenna elements, where N_x^{sat} and N_y^{sat} are the numbers of elements

along the x - and y -axes, respectively. Similarly, each gateway is equipped with the same type of UPA, comprising $N^{\text{gat}} = N_x^{\text{gat}} \times N_y^{\text{gat}}$ elements. Satellite i transmits ISAC signals to detect K airborne targets and communicate with U_i single-antenna UEs. Meanwhile, gateways do not transmit signals but receive reflected echo signals from the targets for cooperative sensing. We assume that UEs are randomly and uniformly distributed within the communication footprint of the serving satellite. The communication footprint is assumed to be non-overlapping with those of other satellites. In contrast, the sensing region is shared by all satellites to enable joint target sensing and is assumed to be disjoint from any communication footprint. The sets of satellites, gateways, UEs served by satellite i , and targets are denoted by $\mathcal{I} = \{1, \dots, I\}$, $\mathcal{L} = \{1, \dots, L\}$, $\mathcal{U}_i = \{1, \dots, U_i\}$, and $\mathcal{K} = \{1, \dots, K\}$, respectively. We also denote the fixed 3D positions of satellite i , gateway l , the u -th UE served by satellite i , and target k as $\mathbf{q}_i^{\text{sat}} = [x_i^{\text{sat}}, y_i^{\text{sat}}, z_i^{\text{sat}}]^T$, $\mathbf{q}_l^{\text{gat}} = [x_l^{\text{gat}}, y_l^{\text{gat}}, z_l^{\text{gat}}]^T$, $\mathbf{q}_{i,u}^{\text{ue}} = [x_{i,u}^{\text{ue}}, y_{i,u}^{\text{ue}}, z_{i,u}^{\text{ue}}]^T$, and $\mathbf{q}_k^{\text{tar}} = [x_k^{\text{tar}}, y_k^{\text{tar}}, z_k^{\text{tar}}]^T$, respectively. It is assumed that the satellite displacement is negligible over the considered time interval due to its short duration. The position information of satellites, gateways, and UEs is perfectly available to all nodes in the network, whereas the positions of targets remain unknown.

A. Channel Model

Typically, the satellite-to-UE channel has a strong line-of-sight (LoS) path and a limited number of weak non-LoS (NLoS) paths due to the high orbital altitude of the satellite. Although the high relative velocity of the satellite induces a Doppler effect, it can be effectively compensated by means of time-frequency synchronization techniques [18]. Motivated by these facts, the communication link between satellite i and the u -th UE associated with satellite j can be modeled as a Rician fading channel [23], which is given by

$$\mathbf{h}_{i,j,u}(t) = \frac{\lambda \sqrt{A_{\text{Tx}}^{\text{sat}} A_{\text{Rx}}^{\text{ue}}}}{4\pi d_{i,j,u}^{\text{sat-ue}}} \left(\sqrt{\frac{\kappa}{1+\kappa}} \mathbf{h}_{i,j,u}^{\text{LoS}} + \sqrt{\frac{1}{1+\kappa}} \mathbf{h}_{i,j,u}^{\text{NLoS}}(t) \right), \quad (1)$$

where λ is the carrier wavelength, $A_{\text{Tx}}^{\text{sat}}$ is the transmit antenna gain of the satellite, $A_{\text{Rx}}^{\text{ue}}$ is the receive antenna gain of the UE, $d_{i,j,u}^{\text{sat-ue}} = \|\mathbf{q}_i^{\text{sat}} - \mathbf{q}_{j,u}^{\text{ue}}\|_2$ denotes the distance between satellite i and the u -th UE associated with satellite j , and κ is the Rician factor. Also, $\mathbf{h}_{i,j,u}^{\text{LoS}} = e^{-j \frac{2\pi d_{i,j,u}^{\text{sat-ue}}}{\lambda}} \mathbf{v}_{i,j,u}^{\text{sat-ue}}$ and $\mathbf{h}_{i,j,u}^{\text{NLoS}}(t) \sim \mathcal{CN}(\mathbf{0}_{N^{\text{sat}}}, \mathbf{I}_{N^{\text{sat}}})$ are the LoS and NLoS components, respectively. Here, the array response vector $\mathbf{v}_{i,j,u}^{\text{sat-ue}} \in \mathbb{C}^{N^{\text{sat}}}$ is constructed based on the AoD of the satellite-to-UE link as follows:

$$\mathbf{v}_{i,j,u}^{\text{sat-ue}} = \mathbf{v}_{x,i,j,u}^{\text{sat-ue}} \otimes \mathbf{v}_{y,i,j,u}^{\text{sat-ue}}, \quad (2)$$

where $\mathbf{v}_{x,i,j,u}^{\text{sat-ue}} \in \mathbb{C}^{N_x^{\text{sat}}}$ and $\mathbf{v}_{y,i,j,u}^{\text{sat-ue}} \in \mathbb{C}^{N_y^{\text{sat}}}$ denote the array responses along the x - and y -axes, respectively. The n -th element of each response is expressed as

$$[\mathbf{v}_{x,i,j,u}^{\text{sat-ue}}]_n = e^{-j\pi(n-1) \cos \phi_{i,j,u}^{\text{sat-ue}}} \cos \theta_{i,j,u}^{\text{sat-ue}}, \quad (3)$$

$$\text{SINR}_{i,u}^{\text{ue}}(t) = \frac{p_{i,u}^c(t) |\mathbf{h}_{i,i,u}^H(t) \mathbf{f}_{i,u}^c(t)|^2}{\sum_{v \in \mathcal{U}_i \setminus \{u\}} p_{i,v}^c(t) |\mathbf{h}_{i,i,u}^H(t) \mathbf{f}_{i,v}^c(t)|^2 + \sum_{j \in \mathcal{I} \setminus \{i\}} \sum_{v \in \mathcal{U}_j} p_{j,v}^c(t) |\mathbf{h}_{j,i,u}^H(t) \mathbf{f}_{j,v}^c(t)|^2 + \sum_{j \in \mathcal{I}} p_j^r(t) |\mathbf{h}_{j,i,u}^H(t) \mathbf{f}_j^r(t)|^2 + \sigma_{i,u}^2}. \quad (11)$$

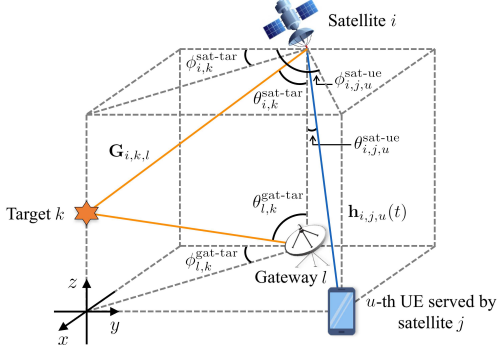


Fig. 2. Channel model of the proposed multi-satellite ISAC network.

$$[\mathbf{v}_{y,i,j,u}^{\text{sat-ue}}]_n = e^{-j\pi(n-1) \sin \phi_{i,j,u}^{\text{sat-ue}} \cos \theta_{i,j,u}^{\text{sat-ue}}}, \quad (4)$$

with the azimuth angle w.r.t. the negative y -axis given by

$$\phi_{i,j,u}^{\text{sat-ue}} = \tan^{-1} \left(-\frac{x_i^{\text{sat}} - x_{j,u}^{\text{ue}}}{y_i^{\text{sat}} - y_{j,u}^{\text{ue}}} \right), \quad (5)$$

and the elevation angle w.r.t. the negative z -axis given by

$$\theta_{i,j,u}^{\text{sat-ue}} = \tan^{-1} \left(\frac{\sqrt{(x_i^{\text{sat}} - x_{j,u}^{\text{ue}})^2 + (y_i^{\text{sat}} - y_{j,u}^{\text{ue}})^2}}{z_i^{\text{sat}} - z_{j,u}^{\text{ue}}} \right). \quad (6)$$

Similarly, the satellite-to-target and target-to-gateway channels are assumed to be dominated by a LoS component due to the lack of scatterers. For point-like targets, the sensing channel from satellite i to gateway l via target k can be expressed as

$$\mathbf{G}_{i,k,l} = \rho_{i,k,l} \sqrt{\frac{\lambda^2 A_{\text{Rx}}^{\text{gat}} A_{\text{Tx}}^{\text{sat}}}{64\pi^3 (d_{l,k}^{\text{gat-tar}})^2 (d_{i,k}^{\text{sat-tar}})^2}} \times e^{-j2\pi \frac{d_{l,k}^{\text{gat-tar}} + d_{i,k}^{\text{sat-tar}}}{\lambda}} \mathbf{v}_{l,k}^{\text{gat-tar}} (\mathbf{v}_{i,k}^{\text{sat-tar}})^H, \quad (7)$$

where $\rho_{i,k,l}$ represents the unknown reflection coefficient of target k over the bistatic path between satellite i and gateway l . According to the Swerling-I model [24], the complex reflection coefficient $\rho_{i,k,l}$ is assumed to be distributed as $\mathcal{CN}(0, \gamma_{i,k,l})$ with radar cross section $\gamma_{i,k,l}$. Here, the receive antenna gain of the gateway is denoted by $A_{\text{Rx}}^{\text{gat}}$, and the distances from gateway l and satellite i to target k are given by $d_{l,k}^{\text{gat-tar}} = \|\mathbf{q}_l^{\text{gat}} - \mathbf{q}_k^{\text{tar}}\|_2$ and $d_{i,k}^{\text{sat-tar}} = \|\mathbf{q}_i^{\text{sat}} - \mathbf{q}_k^{\text{tar}}\|_2$, respectively. As given in (2), the array response vectors for the links from satellite i to target k and from target k to gateway l are denoted by $\mathbf{v}_{i,k}^{\text{sat-tar}} \in \mathbb{C}^{N^{\text{sat}}}$ and $\mathbf{v}_{l,k}^{\text{gat-tar}} \in \mathbb{C}^{N^{\text{gat}}}$, respectively. Note that the elevation angle between gateway l and target k is defined w.r.t. the positive z -axis as

$$\theta_{l,k}^{\text{gat-tar}} = \tan^{-1} \left(-\frac{\sqrt{(x_l^{\text{gat}} - x_k^{\text{tar}})^2 + (y_l^{\text{gat}} - y_k^{\text{tar}})^2}}{z_l^{\text{gat}} - z_k^{\text{tar}}} \right). \quad (8)$$

B. Signal Model

Satellites transmit communication signals jointly with a dedicated sensing signal using a common waveform. The transmitted ISAC signal of satellite i at time t is then given by

$$\mathbf{x}_i(t) = \sqrt{p_i^r(t)} \mathbf{f}_i^r(t) s_i^r(t) + \sum_{u \in \mathcal{U}_i} \sqrt{p_{i,u}^c(t)} \mathbf{f}_{i,u}^c(t) s_{i,u}^c(t), \quad (9)$$

where $p_i^r(t) \geq 0$, $\mathbf{f}_i^r(t) \in \mathbb{C}^{N^{\text{sat}}}$, and $s_i^r(t) \in \mathbb{C}$ represent the sensing signal power, the normalized sensing beamforming vector, and the sensing symbol, respectively. Similarly, the signal power, normalized beamforming vector, and communication symbol used for the u -th UE associated with satellite i are denoted as $p_{i,u}^c(t) \geq 0$, $\mathbf{f}_{i,u}^c(t) \in \mathbb{C}^{N^{\text{sat}}}$, and $s_{i,u}^c(t) \in \mathbb{C}$, respectively. We note that all transmitted communication and sensing symbols are zero-mean, of unit power, and mutually independent.

The received signal of the u -th UE associated with satellite i at time t is expressed as

$$\begin{aligned} y_{i,u}^{\text{ue}}(t) &= \sum_{j \in \mathcal{I}} \mathbf{h}_{j,i,u}^H(t) \mathbf{x}_j(t) + n_{i,u}^{\text{ue}}(t) \\ &= \underbrace{\sqrt{p_{i,u}^c(t)} \mathbf{h}_{i,i,u}^H(t) \mathbf{f}_{i,u}^c(t) s_{i,u}^c(t)}_{\text{Desired signal}} + \underbrace{n_{i,u}^{\text{ue}}(t)}_{\text{AWGN}} \\ &\quad + \underbrace{\sum_{j \in \mathcal{I}} \sqrt{p_j^r(t)} \mathbf{h}_{j,i,u}^H(t) \mathbf{f}_j^r(t) s_j^r(t)}_{\text{Sensing interference}} \\ &\quad + \underbrace{\sum_{j \in \mathcal{I} \setminus \{i\}} \sum_{v \in \mathcal{U}_j} \sqrt{p_{j,v}^c(t)} \mathbf{h}_{j,i,u}^H(t) \mathbf{f}_{j,v}^c(t) s_{j,v}^c(t)}_{\text{Inter-cell interference}} \\ &\quad + \underbrace{\sum_{v \in \mathcal{U}_i \setminus \{u\}} \sqrt{p_{i,v}^c(t)} \mathbf{h}_{i,i,u}^H(t) \mathbf{f}_{i,v}^c(t) s_{i,v}^c(t)}_{\text{Intra-cell interference}}, \end{aligned} \quad (10)$$

where $n_{i,u}^{\text{ue}}(t) \sim \mathcal{CN}(0, \sigma_{i,u}^2)$ is the additive white Gaussian noise (AWGN). We consider the SINR as the performance metric for communication. From (10), the instantaneous SINR of the u -th UE served by satellite i at time t can be obtained as shown in (11) (at the top of this page).

For target sensing, the gateways employ a receive beamforming technique. Then, the echo signal received by gateway l at time t is expressed as

$$y_l^{\text{gat}}(t) = \sum_{k \in \mathcal{K}} \sum_{i \in \mathcal{I}} \mathbf{w}_l^H(t) \mathbf{G}_{i,k,l} \mathbf{x}_i(t) + \mathbf{w}_l^H(t) \mathbf{n}_l^{\text{gat}}(t), \quad (12)$$

where $\mathbf{w}_l(t) \in \mathbb{C}^{N^{\text{gat}}}$ denotes the receive beamforming vector of gateway l , and $\mathbf{n}_l^{\text{gat}}(t) \sim \mathcal{CN}(\mathbf{0}_{N^{\text{gat}}}, \zeta_l^2 \mathbf{I}_{N^{\text{gat}}})$ represents the

AWGN vector. By defining $a_{i,k,l}^{\text{gat}}(t) = \rho_{i,k,l}^{-1} \mathbf{w}_l^H(t) \mathbf{G}_{i,k,l} \mathbf{x}_i(t)$, the echo signal in (12) can be rewritten as

$$y_l^{\text{gat}}(t) = \sum_{k \in \mathcal{K}} \sum_{i \in \mathcal{I}} \rho_{i,k,l} a_{i,k,l}^{\text{gat}}(t) + \mathbf{w}_l^H(t) \mathbf{n}_l^{\text{gat}}(t). \quad (13)$$

III. PROPOSED ISAC BEAMFORMING DESIGN

This section presents the beamforming design for the multi-satellite ISAC network. We focus on a hybrid analog-digital beamforming architecture to provide a more feasible implementation for large-scale antenna arrays [25]. Specifically, satellite i is assumed to employ $U_i + 1$ radio frequency (RF) chains, each connected to N^{sat} phase shifters. Among these, U_i RF chains are allocated for communication, while the remaining RF chain is dedicated to sensing. Similarly, gateway l is equipped with one RF chain to receive only the intended sensing signal. Based on this hybrid architecture, the beamforming design must satisfy the following constraints:

$$|\|\mathbf{w}_l(t)\|_n| = \frac{1}{\sqrt{N^{\text{gat}}}}, \quad l \in \mathcal{L}, t \in \mathcal{T}, n \in \mathcal{N}^{\text{gat}}, \quad (14)$$

$$|\|\mathbf{f}_i^r(t)\|_n| = \frac{1}{\sqrt{N^{\text{sat}}}}, \quad i \in \mathcal{I}, t \in \mathcal{T}, n \in \mathcal{N}^{\text{sat}}, \quad (15)$$

$$|\|\mathbf{f}_{i,u}^c(t)\|_n| = \frac{1}{\sqrt{N^{\text{sat}}}}, \quad i \in \mathcal{I}, u \in \mathcal{U}_i, t \in \mathcal{T}, n \in \mathcal{N}^{\text{sat}}, \quad (16)$$

where $\mathcal{T} = \{1, \dots, T\}$, $\mathcal{N}^{\text{sat}} = \{1, \dots, N^{\text{sat}}\}$ and $\mathcal{N}^{\text{gat}} = \{1, \dots, N^{\text{gat}}\}$. Under these constraints, we first describe a simple grid structure that transforms the continuous sensing problem into a discrete one, which provides a more tractable problem formulation. We then present the proposed designs of the communication and sensing beamforming vectors, respectively.

A. Grid Structure for Efficient Target Sensing

We consider a grid structure in which the 3D sensing region is discretized into M grid points denoted as $\mathbf{q}_m^{\text{grid}} = [x_m^{\text{grid}}, y_m^{\text{grid}}, z_m^{\text{grid}}]^T$ for $m \in \mathcal{M} = \{1, \dots, M\}$. For the m -th grid point, let $a_{i,m,l}^{\text{grid}}(t)$ denote the beamformed sensing channel from satellite i to gateway l via reflection at the m -th grid point at time t without the reflection coefficient. Then, $a_{i,m,l}^{\text{grid}}(t)$ is expressed as

$$a_{i,m,l}^{\text{grid}}(t) = \sqrt{\frac{\lambda^2 A_{\text{Rx}}^{\text{gat}} A_{\text{Tx}}^{\text{sat}}}{64\pi^3 (d_{l,m}^{\text{gat-grid}})^2 (d_{i,m}^{\text{sat-grid}})^2}} e^{-j2\pi \frac{d_{l,m}^{\text{gat-grid}} + d_{i,m}^{\text{sat-grid}}}{\lambda}} \times \mathbf{w}_l^H(t) \mathbf{v}_{l,m}^{\text{gat-grid}} (\mathbf{v}_{i,m}^{\text{sat-grid}})^H \mathbf{x}_i(t), \quad (17)$$

where $d_{l,m}^{\text{gat-grid}} = \|\mathbf{q}_l^{\text{gat}} - \mathbf{q}_m^{\text{grid}}\|_2$ and $d_{i,m}^{\text{sat-grid}} = \|\mathbf{q}_i^{\text{sat}} - \mathbf{q}_m^{\text{grid}}\|_2$ represent the distances from the m -th grid point to gateway l and satellite i , respectively, and the corresponding array response vectors are denoted by $\mathbf{v}_{l,m}^{\text{gat-grid}}$ and $\mathbf{v}_{i,m}^{\text{sat-grid}}$, respectively. It is worth mentioning that $a_{i,m,l}^{\text{grid}}(t)$ is available at both satellites and gateways.

B. Sensing Beamforming Design

The objective of the sensing beamforming design is to enable I satellites and L gateways to probe all M grid points over T time slots. We first introduce a mapping function $\psi: \mathcal{T} \rightarrow \mathcal{M}$, under which the satellites and gateways are configured to probe the $\psi(t)$ -th grid point at time slot t . Without careful beamforming design, the transmitted sensing and communication signals may interfere with each other. To address this issue, the sensing transmit and receive beamforming vectors for the i -th satellite and l -th gateway at time slot t are determined as

$$\mathbf{w}_l(t) = \frac{1}{\sqrt{N^{\text{gat}}}} \mathbf{v}_{l,\psi(t)}^{\text{gat-grid}}, \quad l \in \mathcal{L}, t \in \mathcal{T}, \quad (18)$$

$$\mathbf{f}_i^r(t) = \frac{1}{\sqrt{N^{\text{sat}}}} \mathbf{v}_{i,\psi(t)}^{\text{sat-grid}}, \quad i \in \mathcal{I}, t \in \mathcal{T}, \quad (19)$$

respectively.

We now present Lemma 1 to analyze the performance of the proposed beamforming design.

Lemma 1: Consider a half-wavelength spaced UPA with N_x and N_y elements along the x - and y -axes. Let $\mathbf{v}(\phi, \theta) = \mathbf{v}_x(\phi, \theta) \otimes \mathbf{v}_y(\phi, \theta) \in \mathbb{C}^N$ with $N = N_x N_y$ denote the array steering vector toward azimuth ϕ and elevation θ . Then, for two directions (ϕ_1, θ_1) and (ϕ_2, θ_2) , the crosstalk coefficient between their steering vectors is

$$\frac{|\mathbf{v}(\phi_1, \theta_1)^H \mathbf{v}(\phi_2, \theta_2)|^2}{N} = \frac{1}{N} \left| \frac{\sin(\frac{\pi N_x \delta_x}{2}) \sin(\frac{\pi N_y \delta_y}{2})}{\sin(\frac{\pi \delta_x}{2}) \sin(\frac{\pi \delta_y}{2})} \right|^2, \quad (20)$$

where $\delta_x = \cos \phi_1 \cos \theta_1 - \cos \phi_2 \cos \theta_2$ and $\delta_y = \sin \phi_1 \cos \theta_1 - \sin \phi_2 \cos \theta_2$. Thus, if $(\phi_1, \theta_1) \neq (\phi_2, \theta_2)$ so that $(\delta_x, \delta_y) \neq (0, 0)$, the crosstalk decays to zero as N grows, implying asymptotic orthogonality of distinct steering vectors.

Proof: See [26, (41)]. \blacksquare

This lemma implies that, when the array size is sufficiently large, the proposed beamforming designs in (18) and (19) enable gateways to receive the sensing signals without experiencing significant interference from communication signals. Motivated by this result, we allocate the maximum transmit power to each sensing beamforming vector, i.e., $p_i^r(t) = P_i^r$, $i \in \mathcal{I}, t \in \mathcal{T}$, where P_i^r denotes the maximum sensing power of satellite i , in order to maximize the received sensing signal-to-noise ratio (SNR) of gateways. Note that our design also satisfies the constraints (14) and (15) imposed by the hybrid beamforming architecture.

C. Communication Beamforming Design

Following the same logic as in Sec. III-B, the beamforming vector for the u -th UE served by satellite i is given by

$$\mathbf{f}_{i,u}^c(t) = \frac{1}{\sqrt{N^{\text{sat}}}} \mathbf{v}_{i,i,u}^{\text{sat-ue}}, \quad i \in \mathcal{I}, u \in \mathcal{U}_i, t \in \mathcal{T}. \quad (21)$$

Conventional beamforming schemes such as weighted minimum mean square error [27] and regularized zero-forcing [28], which are known to achieve optimal or near-optimal performance for sum-rate maximization under transmit power constraints, can be applied to downlink multi-user MIMO

$$\underbrace{\begin{bmatrix} \chi_{1,1,1,1}(t) & -\tau_c \chi_{1,1,1,2}(t) & \cdots & -\tau_c \chi_{1,1,I,U_I}(t) \\ -\tau_c \chi_{1,2,1,1}(t) & \chi_{1,2,1,2}(t) & \cdots & -\tau_c \chi_{1,2,I,U_I}(t) \\ \vdots & \vdots & \ddots & \vdots \\ -\tau_c \chi_{I,U_I,1,1}(t) & -\tau_c \chi_{I,U_I,1,2}(t) & \cdots & \chi_{I,U_I,I,U_I}(t) \end{bmatrix}}_{\triangleq \boldsymbol{\chi}(t) \in \mathbb{R}^{U \times U}} \underbrace{\begin{bmatrix} p_{1,1}^c(t) \\ p_{1,2}^c(t) \\ \vdots \\ p_{I,U_I}^c(t) \end{bmatrix}}_{\triangleq \mathbf{p}(t) \in \mathbb{R}^U} = \underbrace{\begin{bmatrix} \tau_c \nu_{1,1}(t) \\ \tau_c \nu_{1,2}(t) \\ \vdots \\ \tau_c \nu_{I,U_I}(t) \end{bmatrix}}_{\triangleq \boldsymbol{\nu}(t) \in \mathbb{R}^U}. \quad (25)$$

systems. However, they are typically designed for fully digital architectures and do not satisfy the hybrid beamforming constraints in (16). For this reason, we adopt a suboptimal beamforming strategy based on the LoS steering vector that satisfies the hybrid beamforming constraints and can mitigate sensing interference, as shown in Lemma 1.

Next, we consider a power allocation problem to minimize the total power consumption under QoS constraints. The power minimization problem for time slot t is formulated as

$$\min_{\{p_{i,u}^c(t)\}_{i \in \mathcal{I}, u \in \mathcal{U}_i}} \sum_{i \in \mathcal{I}} \sum_{u \in \mathcal{U}_i} p_{i,u}^c(t) \quad (22a)$$

$$\text{s.t.} \quad \text{SINR}_{i,u}^{\text{uc}}(t) \geq \tau^c, \quad i \in \mathcal{I}, u \in \mathcal{U}_i, \quad (22b)$$

$$p_{i,u}^c(t) \geq 0, \quad i \in \mathcal{I}, u \in \mathcal{U}_i, \quad (22c)$$

with τ^c representing the SINR threshold for communication. For solving (22), we first rewrite the problem by defining $\chi_{i,u,j,v}(t) = |\mathbf{h}_{j,i,u}^H(t) \mathbf{f}_{j,v}^c(t)|^2$ and $\nu_{i,u}(t) = \sum_{j \in \mathcal{I}} P_j^r |\mathbf{h}_{j,i,u}^H(t) \mathbf{f}_j^r(t)|^2 + \sigma_{i,u}^2$. Applying this, constraint (22b) can be transformed into the following equivalent constraints:

$$p_{i,u}^c(t) \chi_{i,u,i,u}(t) \geq \sum_{j \in \mathcal{I} \setminus \{i\}} \sum_{v \in \mathcal{U}_j} \tau_c p_{j,v}^c(t) \chi_{i,u,j,v}(t) + \tau_c \nu_{i,u}(t) + \sum_{v \in \mathcal{U}_i \setminus \{u\}} \tau_c p_{i,v}^c(t) \chi_{i,u,i,v}(t), \quad (23)$$

for all $i \in \mathcal{I}, u \in \mathcal{U}_i$. Thus, the problem is reformulated as

$$\min_{\{p_{i,u}^c(t)\}_{i \in \mathcal{I}, u \in \mathcal{U}_i}} \sum_{i \in \mathcal{I}} \sum_{u \in \mathcal{U}_i} p_{i,u}^c(t) \quad (24a)$$

$$\text{s.t.} \quad (22c), (23), \quad (24b)$$

which is a standard linear programming (LP) that can be efficiently solved [29].

A feasible and bounded LP always has an optimal solution at a vertex of the feasible polyhedron [30], which implies that the optimal solution to the proposed problem can be achieved when (23) holds with equality. As a result, the optimality condition for problem (24) can be derived as shown in (25) at the top of this page, where $U = \sum_{i \in \mathcal{I}} U_i$. According to the Lévy-Desplanques theorem [31], any strictly diagonally dominant square matrix is non-singular, which means that the matrix $\boldsymbol{\chi}(t)$ is invertible when it satisfies the following conditions:

$$\chi_{i,u,i,u}(t) > \sum_{j \in \mathcal{I} \setminus \{i\}} \sum_{v \in \mathcal{U}_j} \tau_c \chi_{i,u,j,v}(t) + \sum_{v \in \mathcal{U}_i \setminus \{u\}} \tau_c \chi_{i,u,i,v}(t), \quad (26)$$

for all $i \in \mathcal{I}, u \in \mathcal{U}_i$. However, the inequalities in (26) may not always hold, particularly when τ_c is chosen too

large. A practical approach is to adjust the communication SINR threshold to a feasible range. Under this adjustment, the feasibility of problem (24) is guaranteed, and the optimal solution is given by $\mathbf{p}(t) = \boldsymbol{\chi}^{-1}(t) \boldsymbol{\nu}(t)$.

IV. PROPOSED CENTRALIZED MULTI-TARGET SENSING FRAMEWORK

In this section, we present a centralized sensing framework for multi-satellite ISAC networks, where the observations from all gateways are collected and jointly processed to estimate target positions in a 3D region. To this end, we formulate a centralized target sensing problem to exploit the collected observations. We then introduce an OMP-based target sensing algorithm to solve this problem.

A. Centralized Sensing Problem

In practice, centralized processing can be realized by employing a cloud radio access network architecture [32]. In this setup, the observations from distributed gateways are transmitted to the CU and jointly processed. We define $\mathbf{y}_l \in \mathbb{C}^T$ as a sensing observation vector that concatenates the observations at gateway l over T time slots as shown in (27) at the top of page 7. The observation vector \mathbf{y}_l is forwarded to the CU and combined with those from other gateways for joint processing. Stacking the observations of all gateways yields

$$\underbrace{\begin{bmatrix} \mathbf{y}_1 \\ \mathbf{y}_2 \\ \vdots \\ \mathbf{y}_L \end{bmatrix}}_{\triangleq \mathbf{y} \in \mathbb{C}^{TL}} = \underbrace{\begin{bmatrix} \mathbf{A}_1^{\text{gat}} & 0 & \cdots & 0 \\ 0 & \mathbf{A}_2^{\text{gat}} & \cdots & 0 \\ \vdots & \vdots & \ddots & \vdots \\ 0 & 0 & \cdots & \mathbf{A}_L^{\text{gat}} \end{bmatrix}}_{\triangleq \mathbf{A}^{\text{gat}} \in \mathbb{C}^{TL \times KIL}} \underbrace{\begin{bmatrix} \boldsymbol{\rho}_1 \\ \boldsymbol{\rho}_2 \\ \vdots \\ \boldsymbol{\rho}_L \end{bmatrix}}_{\triangleq \boldsymbol{\rho} \in \mathbb{C}^{KIL}} + \underbrace{\begin{bmatrix} \boldsymbol{\omega}_1 \\ \boldsymbol{\omega}_2 \\ \vdots \\ \boldsymbol{\omega}_L \end{bmatrix}}_{\triangleq \boldsymbol{\omega} \in \mathbb{C}^{TL}}. \quad (28)$$

Based on this stacked observation \mathbf{y} , the CU estimates the K unknown target positions $\{\mathbf{q}_k^{\text{tar}}\}_{k \in \mathcal{K}}$. This estimation task can be formulated as a sparse signal recovery problem since only a limited number of targets exist within the discretized search space. We introduce the grid-based sensing matrix $\mathbf{A}^{\text{grid}} \in \mathbb{C}^{TL \times MIL}$ as

$$\mathbf{A}^{\text{grid}} = \text{blkdiag}(\mathbf{A}_1^{\text{grid}}, \dots, \mathbf{A}_L^{\text{grid}}), \quad (29)$$

where $\mathbf{A}_l^{\text{grid}} \in \mathbb{C}^{T \times MI}$ is defined as

$$\mathbf{A}_l^{\text{grid}} = \begin{bmatrix} a_{1,1,l}^{\text{grid}}(1) & \cdots & a_{1,M,l}^{\text{grid}}(1) & \cdots & a_{I,1,l}^{\text{grid}}(1) & \cdots & a_{I,M,l}^{\text{grid}}(1) \\ a_{1,1,l}^{\text{grid}}(2) & \cdots & a_{1,M,l}^{\text{grid}}(2) & \cdots & a_{I,1,l}^{\text{grid}}(2) & \cdots & a_{I,M,l}^{\text{grid}}(2) \\ \vdots & \ddots & \vdots & \ddots & \vdots & \ddots & \vdots \\ a_{1,1,l}^{\text{grid}}(T) & \cdots & a_{1,M,l}^{\text{grid}}(T) & \cdots & a_{I,1,l}^{\text{grid}}(T) & \cdots & a_{I,M,l}^{\text{grid}}(T) \end{bmatrix}. \quad (30)$$

$$\begin{aligned}
\underbrace{\begin{bmatrix} y_l^{\text{gat}}(1) \\ y_l^{\text{gat}}(2) \\ \vdots \\ y_l^{\text{gat}}(T) \end{bmatrix}}_{\triangleq \mathbf{y}_l \in \mathbb{C}^T} &= \underbrace{\begin{bmatrix} a_{1,1,l}^{\text{gat}}(1) & \cdots & a_{1,K,l}^{\text{gat}}(1) & \cdots & a_{T,1,l}^{\text{gat}}(1) & \cdots & a_{T,K,l}^{\text{gat}}(1) \\ a_{1,1,l}^{\text{gat}}(2) & \cdots & a_{1,K,l}^{\text{gat}}(2) & \cdots & a_{T,1,l}^{\text{gat}}(2) & \cdots & a_{T,K,l}^{\text{gat}}(2) \\ \vdots & \ddots & \vdots & \ddots & \vdots & \ddots & \vdots \\ a_{1,1,l}^{\text{gat}}(T) & \cdots & a_{1,K,l}^{\text{gat}}(T) & \cdots & a_{T,1,l}^{\text{gat}}(T) & \cdots & a_{T,K,l}^{\text{gat}}(T) \end{bmatrix}}_{\triangleq \mathbf{A}_l^{\text{gat}} \in \mathbb{C}^{T \times KI}} \underbrace{\begin{bmatrix} \rho_{1,1,l} \\ \vdots \\ \rho_{1,K,l} \\ \vdots \\ \rho_{T,1,l} \\ \vdots \\ \rho_{T,K,l} \end{bmatrix}}_{\triangleq \boldsymbol{\rho}_l \in \mathbb{C}^{KI}} + \underbrace{\begin{bmatrix} \mathbf{w}_l^H(1) \mathbf{n}_l^{\text{gat}}(1) \\ \mathbf{w}_l^H(2) \mathbf{n}_l^{\text{gat}}(2) \\ \vdots \\ \mathbf{w}_l^H(T) \mathbf{n}_l^{\text{gat}}(T) \end{bmatrix}}_{\triangleq \boldsymbol{\omega}_l \in \mathbb{C}^T}. \quad (27)
\end{aligned}$$

Under the assumption of on-grid targets, the stacked observation \mathbf{y} can be rewritten using \mathbf{A}^{grid} as

$$\mathbf{y} = \mathbf{A}^{\text{grid}} \hat{\boldsymbol{\rho}} + \boldsymbol{\omega}, \quad (31)$$

where $\hat{\boldsymbol{\rho}} \in \mathbb{C}^{ML}$ is a sparse vector with KIL non-zero entries. Specifically, if a target is located on the m -th grid point, the corresponding entries are non-zero, i.e., $[\hat{\boldsymbol{\rho}}]_{m+rM} \neq 0$ for each $r \in \mathcal{R} \triangleq \{0, 1, \dots, IL-1\}$. Considering this constraint, we formulate the cooperative target sensing problem that estimates the sparse signal $\hat{\boldsymbol{\rho}}$ from its noisy observation \mathbf{y} as

$$\min_{\hat{\boldsymbol{\rho}}} \|\mathbf{y} - \mathbf{A}^{\text{grid}} \hat{\boldsymbol{\rho}}\|_2^2 \quad (32a)$$

$$\text{s.t.} \quad \sum_{m=1}^M \mathbb{I}[\|\hat{\boldsymbol{\rho}}_m^{\text{group}}\|_0 = IL] = K, \quad (32b)$$

where $\hat{\boldsymbol{\rho}}_m^{\text{group}} = [[\hat{\boldsymbol{\rho}}]_m, [\hat{\boldsymbol{\rho}}]_{m+M}, \dots, [\hat{\boldsymbol{\rho}}]_{m+(IL-1)M}]$ and $\mathbb{I}[\cdot]$ is the indicator function.

In practical environments, it is very unlikely that targets are located exactly on grid points. For this reason, with grid-based parameters, \mathbf{y} can only be approximately represented as

$$\mathbf{y} \approx \mathbf{A}^{\text{grid}} \hat{\boldsymbol{\rho}} + \boldsymbol{\omega}. \quad (33)$$

This mismatch error can be reduced by increasing the grid resolution within the sensing region. However, a larger number of grid points not only increases the complexity of signal recovery, but also reduces its performance by weakening the restricted isometry property [33], [34]. Consequently, the number of grid points should be selected to achieve a desirable trade-off between grid mismatch error and recovery performance degradation.

B. Centralized Sensing Algorithm

The centralized target sensing problem in (32) is NP-hard, as it requires a combinatorial search over all possible sparsity patterns under the constraint in (32b). To avoid the prohibitive complexity of exhaustive search, several efficient algorithms have been developed in the literature [9], [11], [14], [29]. Among these algorithms, we adopt the well-known OMP algorithm as it offers a significant advantage in terms of computational complexity. It should be noted that more advanced sparse recovery algorithms beyond OMP can also be employed to solve (32); however, such methods generally incur higher computational complexity. Moreover, the numerical results in Sec. VI demonstrate that OMP is sufficient to

Algorithm 1 Centralized Sensing Algorithm

Input: \mathbf{y} , \mathbf{A}^{grid} and K .

Output: $\hat{\mathcal{M}}$.

- 1: Initialize $\boldsymbol{\Delta}^{(0)} = \mathbf{y}$, $\hat{\mathcal{M}}^{(0)} = \emptyset$ and $k = 0$.
 - 2: **repeat**
 - 3: $k \leftarrow k + 1$.
 - 4: $\hat{m}_k = \underset{m \in \mathcal{M}}{\text{argmax}} \sum_{r \in \mathcal{R}} |(\boldsymbol{\Delta}^{(k-1)})^H [\mathbf{A}^{\text{grid}}]_{:,m+rM}|$.
 - 5: $\hat{\mathcal{M}}^{(k)} = \hat{\mathcal{M}}^{(k-1)} \cup \{\hat{m}_k\}$.
 - 6: $\mathbf{A}^{(k)} = [[\mathbf{A}^{\text{grid}}]_{:,m+rM}]_{m \in \hat{\mathcal{M}}^{(k)}, r \in \mathcal{R}}$.
 - 7: $\boldsymbol{\Delta}^{(k)} = \mathbf{y} - \mathbf{A}^{(k)} \left((\mathbf{A}^{(k)})^H \mathbf{A}^{(k)} \right)^{-1} (\mathbf{A}^{(k)})^H \mathbf{y}$.
 - 8: **until** $|\hat{\mathcal{M}}^{(k)}| = K$
 - 9: **Return** $\hat{\mathcal{M}} = \hat{\mathcal{M}}^{(k)}$.
-

illustrate the superiority of the proposed sensing framework over the considered baseline schemes.

The fundamental of the OMP algorithm is to iteratively select the column of the measurement matrix that is most correlated with the current residual and update the estimate accordingly. First, we initialize the residual vector as $\boldsymbol{\Delta}^{(0)} = \mathbf{y}$ and the solution set as $\hat{\mathcal{M}}^{(0)} = \emptyset$. At the k -th iteration, the grid point \hat{m}_k most correlated with the current residual is selected as

$$\hat{m}_k = \underset{m \in \mathcal{M}}{\text{argmax}} \sum_{r \in \mathcal{R}} |(\boldsymbol{\Delta}^{(k-1)})^H [\mathbf{A}^{\text{grid}}]_{:,m+rM}|. \quad (34)$$

Then, the solution is updated based on the selected grid point, as $\hat{\mathcal{M}}^{(k)} = \hat{\mathcal{M}}^{(k-1)} \cup \{\hat{m}_k\}$. Subsequently, the residual is updated by subtracting from \mathbf{y} its projection onto the subspace spanned by the selected columns, which is given by

$$\boldsymbol{\Delta}^{(k)} = \mathbf{y} - \mathbf{A}^{(k)} \left((\mathbf{A}^{(k)})^H \mathbf{A}^{(k)} \right)^{-1} (\mathbf{A}^{(k)})^H \mathbf{y}, \quad (35)$$

where $\mathbf{A}^{(k)} = [[\mathbf{A}^{\text{grid}}]_{:,m+rM}]_{m \in \hat{\mathcal{M}}^{(k)}, r \in \mathcal{R}}$. This greedy procedure repeats until a predefined stopping criterion is satisfied. Given prior knowledge of the number of targets, the convergence condition is $|\hat{\mathcal{M}}^{(k)}| = K$; otherwise, it can be stopped when $\|\boldsymbol{\Delta}^{(k)}\|_2 \leq \epsilon$ for a given threshold ϵ . In this study, perfect prior knowledge is assumed to focus the analysis on sensing performance without loss due to target number uncertainty. The details of the proposed algorithm are summarized in Algorithm 1. After executing the above procedure, the estimated positions of the multiple targets are determined as

$$\{\hat{\mathbf{q}}_k^{\text{tar}}\}_{k \in \mathcal{K}} = \{\mathbf{q}_{\hat{m}_k}^{\text{grid}}\}_{\hat{m}_k \in \hat{\mathcal{M}}}. \quad (36)$$

C. Complexity Analysis

The computational complexity of Algorithm 1 is dominated by two parts: the greedy selection in line 4 and the residual update in line 7. At the k -th iteration, inner products between the residual vector of size TL and all MIL columns of the sensing matrix \mathbf{A}^{grid} are computed, whose complexity is $\mathcal{O}(TMIL^2)$. Subsequently, the residual update step entails the computation of $(\mathbf{A}^{(k)})^H \mathbf{A}^{(k)}$ and its inversion, which are on the order of $\mathcal{O}(k^2 TI^2 L^3)$ and $\mathcal{O}(k^3 I^3 L^3)$, respectively. Thus, the overall complexity to solve problem (32) is $\mathcal{O}(KTMIL^2 + K^3 TI^2 L^3 + K^4 I^3 L^3)$. Given that the number of targets is typically much smaller than the grid size (i.e., $K \ll M$), the complexity of Algorithm 1 can be computed as $\mathcal{O}(KTMIL^2)$.

V. PROPOSED DISTRIBUTED MULTI-TARGET SENSING FRAMEWORK

The centralized framework jointly processes observations from all gateways to improve sensing performance. However, this entails substantial fronthaul overhead and high computational complexity. To overcome these limitations, we propose a distributed sensing framework that avoids transmitting raw observations by allowing each gateway to forward only its local sensing results to the CU.

A. Ingredient: Non-Cooperative Sensing at Individual Gateway

As an ingredient for developing the distributed sensing framework, we start by introducing a non-cooperative sensing framework in which target locations are individually estimated by each gateway from its local observations. The non-cooperative sensing problem for gateway l is then formulated as

$$\min_{\hat{\boldsymbol{\rho}}_l \in \mathbb{C}^{MI}} \|\mathbf{y}_l - \mathbf{A}_l^{\text{grid}} \hat{\boldsymbol{\rho}}_l\|_2^2 \quad (37a)$$

$$\text{s.t.} \quad \sum_{m=1}^M \mathbb{I}[\|\hat{\boldsymbol{\rho}}_{l,m}^{\text{group}}\|_0 = I] = K, \quad (37b)$$

where $\hat{\boldsymbol{\rho}}_{l,m}^{\text{group}} = [[\hat{\boldsymbol{\rho}}_l]_m, [\hat{\boldsymbol{\rho}}_l]_{m+M}, \dots, [\hat{\boldsymbol{\rho}}_l]_{m+(I-1)M}]$. The problem in (37) is a group sparse signal recovery problem that can be efficiently, albeit suboptimally, solved using existing sparse recovery algorithms, such as the OMP algorithm [35]. As a concrete example, we adopt OMP to solve (37), following the approach in Sec. IV-B. The detailed steps of the non-cooperative sensing framework are summarized in Algorithm 2.

B. Data Association

In the proposed distributed sensing framework, each gateway constructs a *candidate* set of grid indices for the target locations based on the non-cooperative sensing framework. After this, each gateway forwards the candidate set $\hat{\mathcal{M}}_l$ to the CU for data fusion. The main challenge is how to match the estimates from different gateways to the right target. This is because each gateway provides K potential target positions, but their association with a specific target is unknown.

Algorithm 2 Non-Cooperative Sensing Algorithm

Input: \mathbf{y}_l , $\mathbf{A}_l^{\text{grid}}$ and K .

Output: $\hat{\mathcal{M}}_l$.

- 1: Initialize $\Delta_l^{(0)} = \mathbf{y}_l$, $\hat{\mathcal{M}}_l^{(0)} = \emptyset$ and $k = 0$.
 - 2: **repeat**
 - 3: $k \leftarrow k + 1$.
 - 4: $\hat{m}_{l,k} = \underset{m \in \mathcal{M}}{\operatorname{argmax}} \sum_{i \in \mathcal{I}} |(\Delta_l^{(k-1)})^H [\mathbf{A}_l^{\text{grid}}]_{:,m+(i-1)M}|$.
 - 5: $\hat{\mathcal{M}}_l^{(k)} = \hat{\mathcal{M}}_l^{(k-1)} \cup \{\hat{m}_{l,k}\}$.
 - 6: $\mathbf{A}_l^{(k)} = [[\mathbf{A}_l^{\text{grid}}]_{:,m+(i-1)M}]_{m \in \hat{\mathcal{M}}_l^{(k)}, i \in \mathcal{I}}$.
 - 7: $\Delta_l^{(k)} = \mathbf{y}_l - \mathbf{A}_l^{(k)} \left((\mathbf{A}_l^{(k)})^H \mathbf{A}_l^{(k)} \right)^{-1} (\mathbf{A}_l^{(k)})^H \mathbf{y}_l$.
 - 8: **until** $|\hat{\mathcal{M}}_l^{(k)}| = K$
 - 9: **Return** $\hat{\mathcal{M}}_l = \hat{\mathcal{M}}_l^{(k)}$.
-

For accurate multi-target sensing, we devise a data association process to match the estimates (potentially) associated with the same target. For convenience, we define \mathcal{C}_k as the set of grid indices for target k . The number of elements in \mathcal{C}_k is given by $|\mathcal{C}_k| = L$, since each gateway contributes exactly one estimate. This also implies that if $\hat{m}_{l,k} \in \mathcal{C}_k$, then $\hat{m}_{l,k'} \notin \mathcal{C}_k$ for any $k \neq k'$. Under these constraints, our goal is to find $\mathcal{C}_1, \dots, \mathcal{C}_K$ that minimize the estimation error. The 2D structure of the UPA can provide precise direction of arrival information, but not range information. Thus, the geometry of target k 's possible location as estimated by gateway l is represented by a line passing through the gateway and its estimated position. Based on this geometry, we define the squared Euclidean distance between the line passing through two points $\mathbf{a}, \mathbf{b} \in \mathbb{R}^3$ and a point $\mathbf{c} \in \mathbb{R}^3$ as

$$f(\mathbf{a}, \mathbf{b}, \mathbf{c}) = (\mathbf{c} - \mathbf{a})^T \left(\mathbf{I}_3 - \frac{(\mathbf{b} - \mathbf{a})(\mathbf{b} - \mathbf{a})^T}{\|\mathbf{b} - \mathbf{a}\|^2} \right) (\mathbf{c} - \mathbf{a}). \quad (38)$$

Motivated by this, we formulate the data association problem to minimize the squared distance error, as follows:

$$\min_{\mathcal{C}_1, \dots, \mathcal{C}_K} \sum_{k \in \mathcal{K}} \sum_{l \in \mathcal{L}} \sum_{g \in \mathcal{L} \setminus \{l\}} f(\mathbf{q}_l^{\text{gat}}, \mathbf{q}_{c_{k,l}}^{\text{grid}}, \mathbf{q}_{c_{k,g}}^{\text{grid}}) \quad (39a)$$

$$\text{s.t.} \quad |\mathcal{C}_k| = L, \quad k \in \mathcal{K}, \quad (39b)$$

$$|\mathcal{C}_k \cap \hat{\mathcal{M}}_l| = 1, \quad k \in \mathcal{K}, l \in \mathcal{L}, \quad (39c)$$

$$\bigcup_{k \in \mathcal{K}} \mathcal{C}_k = \bigcup_{l \in \mathcal{L}} \hat{\mathcal{M}}_l, \quad (39d)$$

where $c_{k,l}$ is the element of \mathcal{C}_k corresponding to gateway l . This data association problem is a well-known L -assignment problem. For the case of $L = 2$, it simplifies to a bipartite matching problem, which can be solved by the Hungarian algorithm [36]. The Hungarian algorithm finds an optimal one-to-one correspondence between two sets by iteratively updating a cost matrix. Due to its polynomial-time complexity, it efficiently provides an optimal solution for two-dimensional matching problems. However, when $L \geq 3$, the problem is known to be NP-hard [37], since the bipartite structure no longer holds and the number of possible assignments increases exponentially with L . Practical multi-satellite networks gen-

erally consist of three or more gateways, thereby making the problem intractable. To address this issue, we alternatively solve problem (39) by sequentially applying the Hungarian algorithm.

For solving the data association problem, we first initialize the mapping solution $\mathcal{C}_1, \dots, \mathcal{C}_K$ by assigning one element from the first gateway's estimate $\hat{\mathcal{M}}_1$ to each \mathcal{C}_k , i.e., $\mathcal{C}_1^{(1)} = \{\hat{m}_{1,1}\}$, $\mathcal{C}_2^{(1)} = \{\hat{m}_{1,2}\}$, \dots , $\mathcal{C}_K^{(1)} = \{\hat{m}_{1,K}\}$. At g -th iteration, our objective is to assign $\hat{m}_{g,1}, \hat{m}_{g,2}, \dots, \hat{m}_{g,K}$ to $\mathcal{C}_1^{(j-1)}, \mathcal{C}_2^{(j-1)}, \dots, \mathcal{C}_K^{(j-1)}$, thereby determining $c_{1,g}, c_{2,g}, \dots, c_{K,g}$ so as to minimize the geometric inconsistency with the mapping obtained in the previous iterations. To this end, we introduce a cost matrix $\mathbf{C}^{(g)} \in \mathbb{R}^{K \times K}$, whose (k, k') -th element is defined as

$$\left[\mathbf{C}^{(g)} \right]_{k,k'} = \sum_{l=1}^{g-1} f(\mathbf{q}_l^{\text{gat}}, \mathbf{q}_{\hat{m}_{g,k}}^{\text{grid}}, \mathbf{q}_{c_{k',l}}^{\text{grid}}). \quad (40)$$

We then apply the Hungarian algorithm to $\mathbf{C}^{(g)}$, from which the assignments $c_{1,g}, \dots, c_{K,g}$ are obtained. Consequently, the original problem can be solved by sequentially applying the Hungarian algorithm until the constraint (39b) is satisfied. The detailed procedure of the proposed data association is presented in Algorithm 3. Note that the index k in \mathcal{C}_k is a cluster index determined by the data association algorithm and may not match the true target index. Without loss of generality, we assume that the cluster index k corresponds to target k .

C. Data Fusion

After the data association described above, the CU determines the final estimate for the position of target k from the obtained solution \mathcal{C}_k . To this end, we formulate the distance error minimization problem:

$$\hat{\mathbf{q}}_k^{\text{tar}} = \underset{\mathbf{q} \in \mathbb{R}^3}{\text{argmin}} \sum_{l \in \mathcal{L}} f(\mathbf{q}_l^{\text{gat}}, \mathbf{q}_{c_{k,l}}^{\text{grid}}, \mathbf{q}). \quad (41)$$

To solve this problem, we first rewrite the squared distance as

$$f(\mathbf{q}_l^{\text{gat}}, \mathbf{q}_{c_{k,l}}^{\text{grid}}, \mathbf{q}) = (\mathbf{q} - \mathbf{q}_l^{\text{gat}})^T (\mathbf{I}_3 - \mathbf{q}_{k,l} \mathbf{q}_{k,l}^T) (\mathbf{q} - \mathbf{q}_l^{\text{gat}}), \quad (42)$$

where $\mathbf{q}_{k,l} = (\mathbf{q}_{c_{k,l}}^{\text{grid}} - \mathbf{q}_l^{\text{gat}}) / \|\mathbf{q}_{c_{k,l}}^{\text{grid}} - \mathbf{q}_l^{\text{gat}}\|$. For any vector $\mathbf{d} \in \mathbb{R}^3$, it follows that

$$\mathbf{d}^T (\mathbf{I}_3 - \mathbf{q}_{k,l} \mathbf{q}_{k,l}^T) \mathbf{d} = \|\mathbf{d}\|^2 \sin^2 \alpha, \quad (43)$$

where $\alpha \in [0, \pi]$ denotes the angle between \mathbf{d} and $\mathbf{q}_{k,l}$. Since $\sin^2 \alpha \geq 0$ for all α , we have

$$\mathbf{d}^T (\mathbf{I}_3 - \mathbf{q}_{k,l} \mathbf{q}_{k,l}^T) \mathbf{d} \geq 0, \quad (44)$$

which implies that $\mathbf{I}_3 - \mathbf{q}_{k,l} \mathbf{q}_{k,l}^T$ is a positive semidefinite matrix. Thus, the problem (41) is an unconstrained quadratic program. According to the first-order optimality condition, the optimal solution can be obtained by setting the derivative to zero:

$$\left. \frac{\partial}{\partial \mathbf{q}} \left[\sum_{l \in \mathcal{L}} f(\mathbf{q}_l^{\text{gat}}, \mathbf{q}_{c_{k,l}}^{\text{grid}}, \mathbf{q}) \right] \right|_{\mathbf{q} = \hat{\mathbf{q}}_k^{\text{tar}}} = 2 \sum_{l \in \mathcal{L}} \mathbf{Q}_{k,l} (\hat{\mathbf{q}}_k^{\text{tar}} - \mathbf{q}_l^{\text{gat}}) = 0, \quad (45)$$

Algorithm 3 Clustering of Non-Cooperative Estimates

Input: $\{\hat{\mathcal{M}}_l\}_{l \in \mathcal{L}}$, $\{\mathbf{q}_l^{\text{gat}}\}_{l \in \mathcal{L}}$ and L .

Output: $\{\mathcal{C}_k\}_{k \in \mathcal{K}}$.

- 1: Initialize $\mathcal{C}_1^{(1)} = \{\hat{m}_{1,1}\}$, $\mathcal{C}_2^{(1)} = \{\hat{m}_{1,2}\}$, \dots , $\mathcal{C}_K^{(1)} = \{\hat{m}_{1,K}\}$ and $g = 1$.
 - 2: **repeat**
 - 3: $g \leftarrow g + 1$.
 - 4: Formulate the cost matrix $\mathbf{C}^{(g)}$ as in (40).
 - 5: Apply the Hungarian algorithm to the cost matrix.
 - 6: $\mathcal{C}_k^{(g)} \leftarrow \mathcal{C}_k^{(g-1)} \cup \{c_{k,g}\}$.
 - 7: **until** $|\mathcal{C}_k^{(g)}| = L$
 - 8: **Return** $\mathcal{C}_1 = \mathcal{C}_1^{(g)}$, $\mathcal{C}_2 = \mathcal{C}_2^{(g)}$, \dots , $\mathcal{C}_K = \mathcal{C}_K^{(g)}$.
-

where $\mathbf{Q}_{k,l} = \mathbf{I}_3 - \mathbf{q}_{k,l} \mathbf{q}_{k,l}^T$. As a result, the estimated position of target k under the distributed framework is obtained as

$$\hat{\mathbf{q}}_k^{\text{tar}} = \left(\sum_{l \in \mathcal{L}} \mathbf{Q}_{k,l} \right)^{-1} \left(\sum_{l \in \mathcal{L}} \mathbf{Q}_{k,l} \mathbf{q}_l^{\text{gat}} \right). \quad (46)$$

D. Overall Algorithm

We summarize the overall procedure of the proposed distributed sensing framework. First, each gateway applies Algorithm 2 to locally estimate $\hat{\mathcal{M}}_l$ and forwards the resulting candidate set to the CU. Given $\{\hat{\mathcal{M}}_l\}_{l \in \mathcal{L}}$, the CU performs data association to match the candidates across gateways using the Hungarian algorithm in Algorithm 3. Finally, for each target k , the CU determines the final estimate for the target position using the closed-form solution in (46).

E. Analysis for Complexity and Signaling Overhead

The proposed distributed sensing framework consists of three parts: non-cooperative sensing at each gateway in Algorithm 2, data association at the CU in Algorithm 3, and data fusion based on (46). As discussed in Sec. IV-C, the complexity of Algorithm 2 is calculated as $\mathcal{O}(KTMl + K^3I^2T + K^4I^3)$. Thus, the total complexity of non-cooperative sensing across all L gateways is $\mathcal{O}(L(KTMl + K^3I^2T + K^4I^3))$. Next, the CU performs data association by sequentially applying the Hungarian algorithm. At the g -th iteration, constructing the cost matrix $\mathbf{C}^{(g)}$ in (40) requires the computation of $\sum_{l=1}^{g-1} f(\mathbf{q}_l^{\text{gat}}, \mathbf{q}_{\hat{m}_{g,k}}^{\text{grid}}, \mathbf{q}_{c_{k',l}}^{\text{grid}})$ for each of the K^2 entries, which yields a complexity of $\mathcal{O}(K^2(g-1))$. In addition, the Hungarian algorithm is applied to a $K \times K$ cost matrix, which has a complexity of $\mathcal{O}(K^3)$ [36]. Since this procedure is repeated $L - 1$ times, the overall complexity of the data association stage is $\mathcal{O}(K^2L^2 + K^3L)$. Finally, after obtaining $\{\mathcal{C}_k\}_{k \in \mathcal{K}}$, the CU computes the target position via the closed-form expression in (46). This step involves computing $\sum_{l \in \mathcal{L}} \mathbf{Q}_{k,l}$ and $\sum_{l \in \mathcal{L}} \mathbf{Q}_{k,l} \mathbf{q}_l^{\text{gat}}$ for each k , which scales as $\mathcal{O}(L)$ per target. Since the inversion involves a 3×3 matrix, its cost is constant. Therefore, the computational complexity of data fusion is computed as $\mathcal{O}(KL)$.

TABLE I
SIMULATION PARAMETERS

| Parameter | Value | Parameter | Value |
|------------------------------|----------|------------------|---------------------|
| λ | 0.15 m | κ | 30 dB [23] |
| $A_{\text{Tx}}^{\text{sat}}$ | 30 dBi | N^{sat} | 26×26 |
| $A_{\text{Rx}}^{\text{gat}}$ | 30 dBi | N^{gat} | 32×32 [18] |
| $A_{\text{Rx}}^{\text{ue}}$ | -5.5 dBi | U_i | 5 |
| $\gamma_{i,k,l}$ | 10 dBsm | τ_c | -10 dB |

Combining the above results, the total computational complexity of the distributed sensing framework is $\mathcal{O}(L(KTMl + K^3I^2T + K^4I^3) + K^2L^2 + K^3L + KL)$. Therefore, in practical sensing setups where $K \ll M$ and $K \ll T$, the computational complexity of the distributed framework is on the order of $\mathcal{O}(KTMlL)$, which is lower than $\mathcal{O}(KTMlL^2)$ for the centralized framework. It is worthwhile to mention that the distributed framework requires much lower fronthaul overhead than the centralized framework, since only local sensing results are forwarded to the CU instead of raw observations. Specifically, in the centralized sensing framework, each gateway forwards its raw observation vector \mathbf{y}_l to the CU, which is equivalent to transmitting T complex-valued observations per gateway in each sensing period. In contrast, in the distributed framework, each gateway only transmits the estimated candidate set $\hat{\mathcal{M}}_l$, which consists of only K grid indices. This leads to a considerable reduction in fronthaul overhead, which makes the distributed framework more suitable for practical multi-satellite ISAC systems with limited fronthaul.

VI. NUMERICAL RESULTS

In this section, we evaluate the superiority of the proposed frameworks via simulations. In these simulations, the satellites are located at $\mathbf{q}_1^{\text{sat}} = [50, 50, 600]^T$ km and $\mathbf{q}_2^{\text{sat}} = [-50, -50, 600]^T$ km, and the gateways are deployed at $\mathbf{q}_1^{\text{gat}} = [1, 1, 0]^T$ km, $\mathbf{q}_2^{\text{gat}} = [1, -1, 0]^T$ km, $\mathbf{q}_3^{\text{gat}} = [-1, 1, 0]^T$ km and $\mathbf{q}_4^{\text{gat}} = [-1, -1, 0]^T$ km. The ground UEs are randomly placed within a circular area of 50 km diameter centered at each satellite, with a minimum inter-UE distance of 10 km. We also assume that the airborne targets are uniformly distributed within a circular region of 10 km diameter centered at the origin, and their altitudes are between 17 km and 20 km [38]. We do not consider targets with reflection coefficient magnitudes below 3 because their echo power is too weak for reliable sensing at the assumed SNR level. This sensing region is discretized into $M = 324$ points with a spacing of 1 km. For target sensing, the communication and sensing symbols are independently generated with unit norm and random phases uniformly distributed over $[0, 2\pi)$, and the mapping function is defined as $\psi(t) = ((t - 1) \bmod M) + 1$. The noise power is set as $\sigma_{i,u}^2 = \zeta_l^2 = N_0B$ with the noise power spectral density $N_0 = -174$ dBm/Hz and downlink channel bandwidth $B = 5$ MHz [39]. The remaining parameters are set following 3GPP R1-2401845 [39] and existing studies [18], [23], as summarized in Table I.

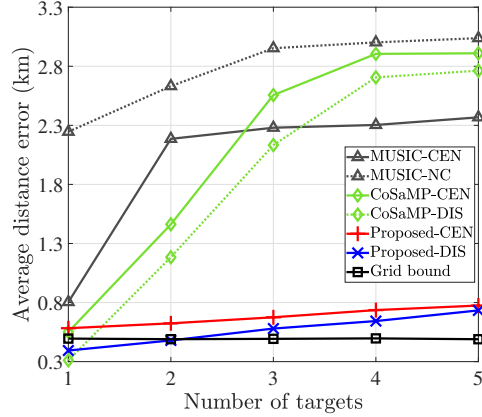


Fig. 3. Average distance error versus the number of targets ($T = M$ and $P_i^r = 5$ W).

We consider the average distance error as the sensing performance metric, which is defined as $\frac{1}{K} \sum_{k \in \mathcal{K}} \|\mathbf{q}_k^{\text{tar}} - \hat{\mathbf{q}}_k^{\text{tar}}\|_2$. The communication performance is also evaluated via the average transmit power, which is calculated as $\frac{1}{T} \sum_{t \in \mathcal{T}} \sum_{i \in \mathcal{I}} \sum_{u \in \mathcal{U}_i} p_{i,u}^c(t)$. All simulation results are averaged over 1000 random samples.

For performance comparisons, the following benchmark schemes are considered.

- **Proposed-CEN and Proposed-DIS:** The proposed centralized and distributed sensing frameworks described in Secs. IV and V, respectively.
- **OMP-NC:** The non-cooperative sensing framework summarized in Algorithm 2, which only uses the first gateway and then applies the OMP method.
- **MUSIC-CEN and MUSIC-NC:** The classical MUSIC algorithm [40] implemented with one satellite and either four gateways (centralized) or a single gateway (non-cooperative), where the sensing power is set to $P_i^r I$ and the number of time slots is $10M$. In the centralized case, the MUSIC pseudo-spectrum is defined as $1 / \sum_{l \in \mathcal{L}} (\mathbf{v}_{l,m}^{\text{gat-grid}})^H \mathbf{U}_l \mathbf{U}_l^H \mathbf{v}_{l,m}^{\text{gat-grid}}$, where \mathbf{U}_l denotes the noise subspace obtained from the sample covariance matrix of the received signals at gateway l .
- **CoSaMP-CEN and CoSaMP-DIS:** Variants of the proposed centralized and distributed sensing frameworks, where compressive sampling matching pursuit (CoSaMP) [41] is applied for sparse signal recovery, instead of OMP.
- **OMP-DIS + K-means:** A distributed sensing framework in which K -means clustering [42] is applied for data association instead of the Hungarian algorithm. At each iteration, K -means clustering is applied to the local sensing results to extract one target location.
- **Grid bound:** The average distance between the true target location and its nearest grid point, which is a performance bound for grid-based search methods.

Fig. 3 plots the average distance error versus the number of targets. The figure shows that both the proposed centralized and distributed frameworks outperform other performance

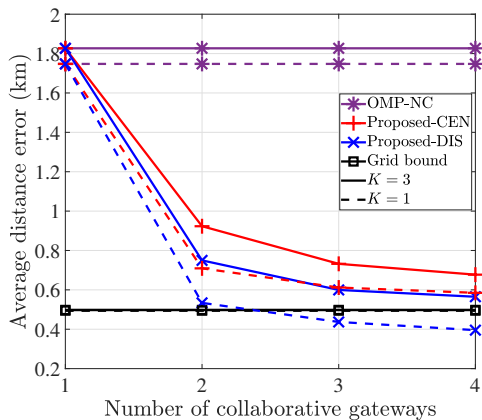


Fig. 4. Average distance error versus the number of collaborative gateways ($T = M$ and $P_i^r = 1$ W).

baselines. The figure also shows that the distributed framework consistently outperforms the centralized framework across all regions, despite requiring substantially lower fronthaul overhead and computational complexity. Specifically, in the single-target case, the distributed framework surpasses the grid bound, owing to its ability to resolve off-grid targets through data fusion. On the contrary, the centralized framework is restricted to on-grid estimation and is therefore bounded by the grid error.

Compared to the compressed sensing benchmark, the OMP-based algorithm achieves more accurate sensing performance in multi-target scenarios. For CoSaMP, off-grid basis mismatch spreads target energy over coherent atoms, resulting in incorrect pruning and performance loss. The MUSIC algorithm can provide precise AoD information, but not range information. For this reason, centralized MUSIC achieves better performance than the non-cooperative one; however, it still shows a larger error compared to the proposed frameworks.

Fig. 4 plots the average distance error versus the number of collaborative gateways. As shown in Fig. 4, the performance of the proposed frameworks improves significantly as more gateways cooperate for sensing. In contrast, the non-cooperative framework does not exhibit such performance gains, as it relies solely on individual sensing without cooperation. The distributed framework consistently outperforms the centralized framework across all regions, which is consistent with the results shown in Fig. 3.

Fig. 5 shows the snapshots of the sensing results of the non-cooperative sensing framework (OMP-NC) obtained from the first to fourth gateways. As shown in Fig. 5, the non-cooperative sensing framework can provide accurate angular information; however, it exhibits poor performance in estimating the target range. This is because the two-dimensional structure of the UPA primarily captures angular information. Consequently, each gateway tends to select the nearest grid points with the same angular direction as the target to achieve higher correlation. For this reason, post-processing is required to compensate for the inaccurate range information, as done in the proposed distributed framework.

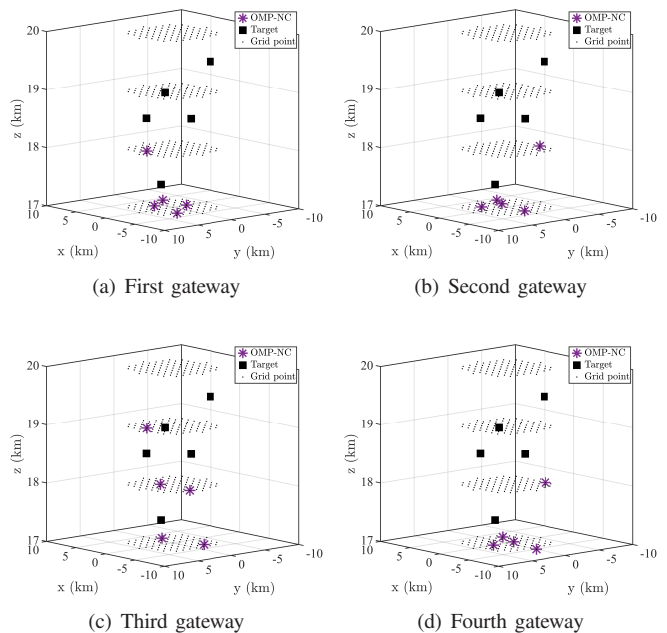


Fig. 5. Snapshots of the sensing results of the non-cooperative sensing framework (OMP-NC) obtained from the first to fourth gateways ($K = 5$, $T = M$, and $P_i^r = 1$ W).

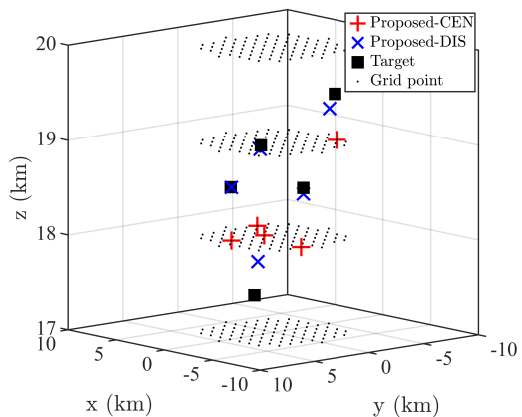
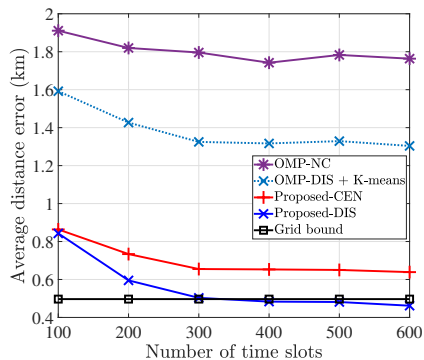
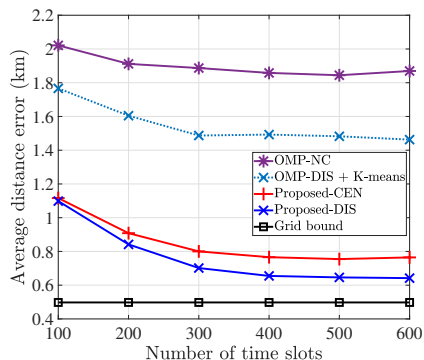


Fig. 6. Snapshots of the sensing results of the proposed centralized and distributed frameworks for the scenario considered in Fig. 5 ($K = 5$, $T = M$, and $P_i^r = 1$ W).

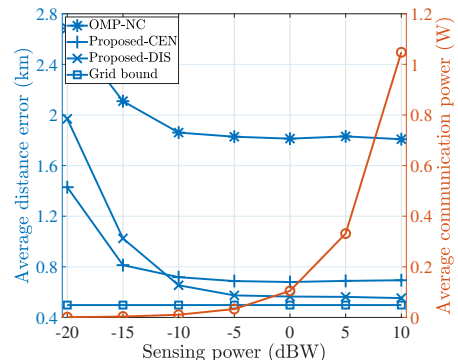
Fig. 6 shows the snapshots of the sensing results of the proposed centralized and distributed frameworks for the scenario considered in Fig. 5. Compared with non-cooperative sensing, both the centralized and distributed frameworks achieve improved estimation accuracy by combining raw observations or local sensing results from multiple gateways. Notably, even if the distributed framework fuses inaccurate estimates (see Fig. 5), it still attains better sensing performance than the centralized framework. This result verifies the effectiveness of the proposed data association and fusion mechanisms.

Fig. 7 depicts the average distance error versus the number of time slots. We first observe that an increased number of time slots is beneficial for all schemes. This is because more observations enhance measurement diversity, thereby

(a) $K = 2$ (b) $K = 4$ Fig. 7. Average distance error versus the number of time slots ($P_i^r = 1$ W).

improving the accuracy of target estimation. Moreover, K -means clustering provides a noticeable improvement over the non-cooperative sensing scheme by grouping locally estimated target locations. However, this improvement is smaller than that from the proposed distributed framework. This is because K -means clustering is based on Euclidean distance, which is not suitable for the 2D UPA structure that mainly provides AoD information. In contrast, Algorithm 3 utilizes angular information via the Hungarian algorithm, which provides more effective clustering of local estimates. We also note that, for $K = 2$, the performance of the proposed distributed framework is comparable to that of the grid bound given a sufficient number of time slots.

Fig. 8 plots the average distance error and average communication power versus sensing power. The communication power consumption increases with the sensing power. This is because sensing signals interfere with the downlink transmission for ground UEs, thereby requiring additional transmit power to satisfy the SINR constraints. It is also observed that the centralized framework achieves the best performance in the low sensing power regime, as jointly processing raw observations is more effective under low SNR conditions. As the sensing power increases, the distributed framework improves significantly and surpasses the centralized one due to more reliable local estimation and effective data fusion. For all schemes, the distance error decreases with sensing

Fig. 8. Average distance error and average communication power versus sensing power ($K = 3$ and $T = M$).

power but saturates beyond a certain level, since structural factors such as grid resolution and basis mismatch constitute the dominant performance bottleneck rather than noise. These results highlight the sensing-communication trade-off, where higher sensing power enhances accuracy at the cost of increased communication power consumption.

VII. CONCLUSION

In this paper, we have investigated a downlink multi-satellite ISAC network, where multiple satellites and gateways are deployed to simultaneously provide communication services to ground UEs and perform airborne target sensing. We developed centralized and distributed sensing frameworks based on a practical hybrid analog-digital beamforming architecture. Under the centralized sensing framework, all gateways forward their observations to a CU, and then the collected data are jointly processed using group sparse recovery algorithms. Conversely, under the distributed framework, each gateway individually estimates the target positions and forwards its results to the CU. For data association with the right targets, we proposed a data association method that sequentially applies the Hungarian algorithm. After the association, the target positions are estimated using a closed-form solution to the optimal distance error minimization problem. Through simulations, we demonstrated the superiority of the proposed frameworks over existing sensing frameworks while guaranteeing communication performance. We also analyzed the sensing-communication trade-off from the viewpoints of sensing accuracy and communication power consumption under the proposed frameworks.

For further work in this area, a robust design with hardware impairments, such as imperfect synchronization [14] and phase noise [43], can be explored. In addition, comparisons between model-driven methods and learning techniques can also be studied in cooperative multi-satellite ISAC networks.

REFERENCES

- [1] O. Kodheli, E. Lagunas, N. Maturo, S. K. Sharma, B. Shankar, J. F. M. Montoya, J. C. M. Duncan, D. Spano, S. Chatzinotas, S. Kisseleff *et al.*, "Satellite communications in the new space era: A survey and future challenges," *IEEE Commun. Surveys Tuts.*, vol. 23, no. 1, pp. 70–109, 4th Quart. 2021.

- [2] S. Jeon, S. Kim, G. Im, and Y.-S. Jeon, "Beam-hopping pattern design for grant-free random access in LEO satellite communications," *IEEE Trans. Wireless Commun.*, vol. 25, pp. 8246–8259, Jan. 2026.
- [3] T. Darwish, G. K. Kurt, H. Yanikomeroglu, M. Bellemare, and G. Lamontagne, "LEO satellites in 5G and beyond networks: A review from a standardization perspective," *IEEE Access*, vol. 10, pp. 35 040–35 060, 2022.
- [4] Y. He, C. Wang, C. Qi, and Z. Feng, "Spatial ultra-sparse distributed antenna satellite-ground cooperative transmission architecture: Challenges, key technologies, and trends," *IEEE Commun. Mag.*, vol. 62, no. 9, pp. 136–143, Sep. 2024.
- [5] I. Del Portillo, B. G. Cameron, and E. F. Crawley, "A technical comparison of three low Earth orbit satellite constellation systems to provide global broadband," *Acta Astronautica*, vol. 159, pp. 123–135, Jun. 2019.
- [6] S. Liu, Z. Gao, Y. Wu, D. W. K. Ng, X. Gao, K.-K. Wong, S. Chatzinotas, and B. Ottersten, "LEO satellite constellations for 5G and beyond: How will they reshape vertical domains?" *IEEE Commun. Mag.*, vol. 59, no. 7, pp. 30–36, Jul. 2021.
- [7] L. Yin, Z. Liu, M. B. Shankar, M. Alae-Kerahroodi, and B. Clerckx, "Integrated sensing and communications enabled low Earth orbit satellite systems," *IEEE Netw.*, vol. 38, no. 6, pp. 252–258, Nov. 2024.
- [8] Z. Wei, H. Qu, Y. Wang, X. Yuan, H. Wu, Y. Du, K. Han, N. Zhang, and Z. Feng, "Integrated sensing and communication signals toward 5G-A and 6G: A survey," *IEEE Internet Things J.*, vol. 10, no. 13, pp. 11 068–11 072, Jul. 2023.
- [9] Q. Shi, L. Liu, S. Zhang, and S. Cui, "Device-free sensing in OFDM cellular network," *IEEE J. Sel. Areas Commun.*, vol. 40, no. 6, pp. 1838–1853, Jun. 2022.
- [10] K. Meng, C. Masouros, A. P. Petropulu, and L. Hanzo, "Cooperative ISAC networks: Opportunities and challenges," *IEEE Wireless Commun.*, vol. 32, no. 3, pp. 212–219, Jun. 2025.
- [11] T. Yang, S. Li, Y. Song, K. Zhi, and G. Caire, "Cooperative multistatic target detection in cell-free communication networks," in *Proc. IEEE Wireless Commun. Netw. Conf.*, Mar. 2025, pp. 1–6.
- [12] M. Nozari, I. Leyva-Mayorga, F. Saggese, and G. Berardinelli, "Toward ISAC-empowered subnetworks: Cooperative localization and iterative node selection," arXiv preprint arXiv:2511.12348, 2025.
- [13] S. Lyu, X. Hu, C. Liu, and M. Peng, "IRS-aided location sensing and beamforming in ISAC systems: Distributed or not?" *IEEE Trans. Veh. Technol.*, vol. 73, no. 9, pp. 13 219–13 233, Sep. 2024.
- [14] Q. Shi and L. Liu, "Joint LOS identification and data association for 6G-enabled networked device-free sensing," *IEEE Trans. Commun.*, vol. 72, no. 8, pp. 5117–5129, Aug. 2024.
- [15] X. Lou, W. Xia, S. Jin, and H. Zhu, "Beamforming optimization in distributed ISAC system with integrated active and passive sensing," *IEEE Trans. Commun.*, vol. 73, no. 3, pp. 1607–1620, Mar. 2025.
- [16] L. You, X. Qiang, C. G. Tsinos, F. Liu, W. Wang, X. Gao, and B. Ottersten, "Beam squint-aware integrated sensing and communications for hybrid massive MIMO LEO satellite systems," *IEEE J. Sel. Areas Commun.*, vol. 40, no. 10, pp. 2994–3009, Oct. 2022.
- [17] Q. Kong, L. You, H. Li, H. Zhou, Y. Wang, F. Zhu, and X. Gao, "Cooperative precoding for integrated sensing and communication in massive MIMO LEO satellite-terrestrial networks," *IEEE Wireless Commun. Lett.*, vol. 14, no. 12, pp. 4117–4121, Dec. 2025.
- [18] J. Park, J. Seong, Y. Mao, W. Shin, and B. Ottersten, "A bistatic ISAC framework for LEO satellite systems: A rate-splitting approach," *IEEE Trans. Aerosp. Electron. Syst.*, vol. 61, no. 6, pp. 17 282–17 301, Dec. 2025.
- [19] J. Liu, C. Ma, X. Tang, F. Wang, S. Wang, and W. Xu, "An efficient integrated communication-navigation signal scheme based on OFDM for LEO satellites networks," *IEEE Internet Things J.*, vol. 13, no. 1, pp. 361–376, Jan. 2026.
- [20] Y. Wang, Y. Chen, Y. Qiao, H. Luo, X. Wang, R. Li, and J. Wang, "Cooperative beam hopping for accurate positioning in ultra-dense LEO satellite networks," in *Proc. IEEE Int. Conf. Commun. Workshops*, May 2021, pp. 1–6.
- [21] H. Xv, Y. Sun, Y. Zhao, M. Peng, and S. Zhang, "Joint beam scheduling and beamforming design for cooperative positioning in multi-beam LEO satellite networks," *IEEE Trans. Veh. Technol.*, vol. 73, no. 4, pp. 5276–5287, Apr. 2024.
- [22] Q. Wang, X. Chen, Q. Qi, M. Li, and W. Gerstacker, "Multiple-satellite cooperative information communication and location sensing in LEO satellite constellations," *IEEE Trans. Wireless Commun.*, vol. 24, no. 4, pp. 3346–3361, Apr. 2025.
- [23] S. Yoo, S. Jeong, J. Kim, and J. Kang, "Cache-assisted mobile-edge computing over space-air-ground integrated networks for extended reality applications," *IEEE Internet Things J.*, vol. 11, no. 10, pp. 18 306–18 319, May 2024.
- [24] M. A. Richards, *Fundamentals of Radar Signal Processing*. New York, NY, USA: McGraw-Hill, 2014.
- [25] A. F. Molisch, V. V. Ratnam, S. Han, Z. Li, S. L. H. Nguyen, L. Li, and K. Haneda, "Hybrid beamforming for massive MIMO: A survey," *IEEE Commun. Mag.*, vol. 55, no. 9, pp. 134–141, Sep. 2017.
- [26] J. Chen, "When does asymptotic orthogonality exist for very large arrays?" in *Proc. IEEE Global Commun. Conf.*, Dec. 2013, pp. 4146–4150.
- [27] S. S. Christensen, R. Agarwal, E. De Carvalho, and J. M. Cioffi, "Weighted sum-rate maximization using weighted MMSE for MIMO-BC beamforming design," *IEEE Trans. Wireless Commun.*, vol. 7, no. 12, pp. 4792–4799, Dec. 2008.
- [28] C. B. Peel, B. M. Hochwald, and A. L. Swindlehurst, "A vector-perturbation technique for near-capacity multiantenna multiuser communication-part I: Channel inversion and regularization," *IEEE Trans. Commun.*, vol. 53, no. 1, pp. 195–202, Jan. 2005.
- [29] J. Jo, J. Park, Y.-S. Jeon, and H. V. Poor, "Beam-squint-aided hierarchical sensing for integrated sensing and communications with uniform planar arrays," *IEEE Trans. Wireless Commun.*, vol. 25, pp. 12 740–12 753, Mar. 2026.
- [30] S. Boyd and L. Vandenberghe, *Convex Optimization*. Cambridge, U.K.: Cambridge Univ. Press, 2004.
- [31] R. A. Horn and C. R. Johnson, *Matrix Analysis*. Cambridge, U.K.: Cambridge Univ. Press, 2012.
- [32] O. Simeone, A. Maeder, M. Peng, O. Sahin, and W. Yu, "Cloud radio access network: Virtualizing wireless access for dense heterogeneous systems," *J. Commun. Netw.*, vol. 18, no. 2, pp. 135–149, Apr. 2016.
- [33] N. T. Nguyen, V.-D. Nguyen, H. V. Nguyen, H. Q. Ngo, A. L. Swindlehurst, and M. Juntti, "Performance analysis and power allocation for massive MIMO ISAC systems," *IEEE Trans. Signal Process.*, vol. 73, pp. 1691–1707, Mar. 2025.
- [34] Y. C. Eldar and G. Kutyniok, *Compressed Sensing: Theory and Applications*. Cambridge, U.K.: Cambridge Univ. Press, 2012.
- [35] Y. C. Pati, R. Rezaifar, and P. S. Krishnaprasad, "Orthogonal matching pursuit: Recursive function approximation with applications to wavelet decomposition," in *Proc. 27th Asilomar Conf. Signals, Syst. Comput.*, Nov. 1993, pp. 40–44.
- [36] H. W. Kuhn, "The Hungarian method for the assignment problem," *Nav. Res. Logistics Quart.*, vol. 2, no. 1-2, pp. 83–97, Mar. 1955.
- [37] A. M. Frieze, "Complexity of a 3-dimensional assignment problem," *Eur. J. Oper. Res.*, vol. 13, no. 2, pp. 161–164, Jun. 1983.
- [38] A. K. Widiawan and R. Tafazolli, "High altitude platform station (HAPS): A review of new infrastructure development for future wireless communications," *Wireless Pers. Commun.*, vol. 42, no. 3, pp. 387–404, Aug. 2007.
- [39] 3GPP R1-2404204, "FL Summary 3: NR-NTN downlink coverage enhancements," May 2024.
- [40] R. Schmidt, "Multiple emitter location and signal parameter estimation," *IEEE Trans. Antennas Propag.*, vol. AP-34, no. 3, pp. 276–280, Mar. 1986.
- [41] D. Needell and J. A. Tropp, "CoSaMP: Iterative signal recovery from incomplete and inaccurate samples," *Appl. Comput. Harmon. Anal.*, vol. 26, no. 3, pp. 301–321, May 2009.
- [42] J. MacQueen, "Some methods for classification and analysis of multivariate observations," in *Proc. 5th Berkeley Symp. Math. Statist. Probab.*, Jan. 1967, pp. 281–297.
- [43] H. Dong and O. B. Akan, "Fundamental limits of THz inter-satellite ISAC under hardware impairments," arXiv preprint arXiv:2509.15902, 2025.